Research Square

Preprints are preliminary reports that have not undergone peer review.
They should not be considered conclusive, used to inform clinical practice,
or referenced by the media as validated information.

Self-Assembly of Silver Clusters into One- and Two-Dimensional Structures as Artificial Intelligent Sensors of Alcohol

Gao Li (gaoli@dicp.ac.cn)
Dalian Institute of Chemical Physics https://orcid.org/0000-0001-6649-5796
Zhaoxian Qin
Dalian Institute of Chemical Physics https://orcid.org/0000-0001-8651-7091
Sachil Sharma
Dalian Institute of Chemical Physics
Yongwu Peng
Zhejiang University of Technology

Article

Keywords: silver cluster-based polymers, Ag-CBPs, artificial intelligence

Posted Date: November 3rd, 2021

DOI: https://doi.org/10.21203/rs.3.rs-964647/v1

License: This work is licensed under a Creative Commons Attribution 4.0 International License.
Read Full License

Self-Assembly of Silver Clusters into One- and Two-Dimensional Structures as Artificial Intelligent Sensors of Alcohol

Author Information

Affiliations

State Key Laboratory of Catalysis, Dalian Institute of Chemical Physics, Chinese Academy of Sciences, Dalian 116023, China

Zhaoxian Qin, Sachil Sharma & Gao Li

College of Materials Science and Engineering and College of Chemical Engineering, Zhejiang University of Technology, Hangzhou 310014, China

Yongwu Peng

University of Chinese Academy of Sciences, Beijing 100049, China

Zhaoxian Qin & Gao Li

Z, Qin and S. Sharma contribute to this work equally.

Contributions

G. L. conceived the work. Z. Q., S. S. and Y. P. performed the experiments. Z. Q., S. S. and G. L. wrote the manuscript. All authors discussed the results and commented on the manuscript.

Corresponding author

Correspondence to: Gao Li (gaoli@dicp.ac.cn), ORCID ID: 0000-0001-6649-5796

Abstract

Reggeization and response to external stimulus is an important part of artificial intelligence, which would significantly improve the quality of life in the future. The development of new materials for the design of sensitive and responsive sensors has become a crucial component. Here, two silver cluster-based

polymers (Ag-CBPs), including one-dimensional (1D) $\{Ag_{22}(L1)_8(CF_3CO_2)_{14}(CH_3OH)_2\}_n$ chain and two-dimensional (2D) $\{[Ag_{12}(L2)_2(CO_2CF_3)_{14}(H_2O)_4(AgCO_2CF_3)_4](HNEt_3)_2\}_n$ film, are designed and used to simulate the human nose—an elegant sensor to smells, to distinguish organic solvents. We study the relationship between the atomic structures of Ag-CBPs determined by X-ray diffraction and electrical properties in the presence of organic solvents (e.g. methanol, ethanol). The ligands, cations and the ligated solvent molecules not only play an important role in the self-assembly process of Ag-CBP materials, but also determine their physiochemical properties. An application of cluster-based polymers is demonstrated in the artificial intelligent sensors.

Introduction

The emerging artificial intelligence technology based on big data collected by various sensors is becoming a hot topic, which also boosts the demand for new multifunctional materials in order to design highly sensitive and high-precision sensors. The precise, selective, and swift measurement of volatile alcohols is of critical importance in various areas such as the food industry,[1,2] occupational safety,[3] and forensics.[4,5] In this direction, the multi-dimensional nanoscale materials have garnered a lot of attention owing to their peculiarity in structures and properties, such as atomic/molecular thickness, optical transparency and large surface areas.[6,7] The fabrication of alcohol sensing devices is an important aspect for the application of these materials. For instance, graphene-based nanomaterials are considered as the frontier of investigated sensing materials.[8-11] And the changes in conductivity of graphene-based materials upon the adsorption of gas molecules lead to the gas detection. Besides this, some other two-dimensional materials including nanostructures based on metal oxides,[12,13] nanoporous silicon,[14] hybrid carbon-based nanostructures,[15] metal organic frameworks (MOFs),[16] and hybrids of fiber optics with nanostructures[17] have also displayed great promise in sensing of the alcohols.

Recently, the burgeoning metal nanoclusters with well resolved-crystal structures show great prospect in fundamental researches and applications in various aspects including luminescence, medicine, catalysis, energy, and biology[18-24] owing to their unique physiochemical properties originated from

structures. Meanwhile, multi-dimensional (e.g. 1D,[26-29] 2D,[27,30-34] and 3D[30,35-42]) self-assembled structures of metal clusters have recently been designed to tailor their properties. Mak and co-workers have made enormous contribution on the synthesis and structural determination of multidimensional silver nanocluster-based materials.[30-32] Sun et al. have reported a series of multi-dimensional self-assembled nanocluster-based clusters with polyoxometallate (POM) as an anion template, where organic ligands and halide atoms were used as linkers to connect clusters.[36,37] Zhu and co-workers synthesized two 3D structures comprised of $[Au_1Ag_{22}(SAdm)_{12}](SbF_6)_2Cl$ and $[Au_1Ag_{22}(SAdm)_{12}](SbF_6)_3$ (SAdm = adamantanethiolate) as structural units.[35] These metal cluster-based materials have been well-developed as fluorescence probes to detect organic compounds[23-24] due to their unique fluorescence properties. However, the study of metal cluster-based materials applied as electrochemical sensors is still quite rare so far.

Herein, we present the synthesis of two novel silver cluster-based polymers (Ag-CBPs) with atomically precise structures, including $\{Ag_{22}(L1)_8(CF_3CO_2)_{14}(CH_3OH)_2\}_n$ (L1 = 3-(prop-2-yn-1-yloxy)-benzonitrile) chains and $\{[Ag_{12}(L2)_2(CO_2CF_3)_{14}(H_2O)_4(AgCO_2CF_3)_4]\text{-}(HNEt_3)_2\}_n$ (L2 = 1-(3-mercaptoprop-1-en-2-yl)-2-methoxypyridin-1-ium) film (abbreviated as Ag_{22}-CBP and Ag_{16}-CBP, respectively, for clarity hereafter), which are determined by single crystal X-ray diffraction. Interestingly, they show different conductivity under an external voltage in the presence of different organic solvents, which is proved to be related to their structural differences. We further find that the charge transfer and the species of carriers have an important influence on the conductivity of Ag-CBPs. The different responses of Ag-CBPs with the variation of organic solvents hold promise in the design of artificial intelligent sensors to distinguish solvents like the nose to differentiate various smells.

Results

Preparation and structure determination of Ag-CBPs. The cluster-based polymeric materials in this study with compositions of Ag_{22}-CBP and Ag_{16}-CBP were synthesized through a bottom-up synthetic strategy. Briefly, these polymeric materials were produced by the reaction and self-assembly of the

corresponding silver precursors (Ag-L1 and Ag-L2) with $AgCO_2CF_3$, respectively (see SI for details). Here the alkynylate and thiolate ligands are selected to construct highly stable Ag-CBPs for their strong interaction and the flexible coordination between ligands and Ag atoms.[31,43]

The compositions and atomic structures of the Ag-CBPs are determined by single crystal X-ray diffraction (SCXRD). The Ag_{22}-CBP crystallizes in the *C2/c* space group. The minimum asymmetry unit of Ag_{22}-CBP is constructed by four ingredients, including 11 Ag atoms, 7 trifluoroacetate anions, 4 L1 anions, and a methanol molecule, as depicted in Fig. 1a. An asymmetry unit rotates 180 ^{o} around a C_2 axis forming the monomer in Ag_{22}-CBP (Fig. 1b). And thus, a metal framework constructed by 22 Ag atoms is furnished in a monomer, where the distances between the silver atoms range from 2.798(4) Å to 3.353(3) Å. The monomers connect with each other in a head to tail manner, giving a 1D silver chain along ***c***-axis (Fig. 1c) through Ag-Ag bonds (3.302(4) Å), Ag-O-C(CF_3)-O-Ag and Ag-$O_{trifluoroacetate}$-Ag motifs, and Ag-alkynylate bonds (Supplementary Figure 1), which looks like the millipede in nature. The obtained silver chains are covered by L1 ligands and trifluoroacetate ions through various bonds. For the L1 ligands, both the terminal C≡C and C≡N groups are bonded to Ag atoms (Supplementary Figure 2). Three types of coordination modes of terminal C≡C group are observed: (i) the μ_4-η^1, η^1, η^2, η^2 mode (Supplementary Figure 3a), in which the C≡C group bonds to two Ag atoms via σ-bond and to another two Ag atoms through π-bond; (ii) the μ_5-η^1, η^1, η^1 η^2, η^2 mode (Supplementary Figure 3b), in which the C≡C group links to three Ag atoms via σ-bond and to another two Ag atoms through π-bond; and (iii) the μ_4-η^1, η^1, η^1, η^2 mode (Supplementary Figure 3c), in which the C≡C group bond to three Ag atoms via σ-bond and to another Ag atom through π-bond. Only the C≡N-Ag σ-bonding mode is detected between the C≡N group and Ag, Supplementary Figure 2. Besides, three coordination modes are observed between trifluoroacetate ions and Ag atoms, namely, μ_1-$O_{trifluoroacetate}$, μ_2-$O_{trifluoroacetate}$, and μ_3-$O_{trifluoroacetate}$ bonding modes. Besides L1 ligands and trifluoroacetate ions, it is worth noting that the non-ionized methanol molecules bind with Ag atoms through Ag-$O_{methanol}$ bond (2.425(2) Å), which is shorter than the Ag-$O_{trifluoroacetate}$ bonds in length (2.688(5) Å), Fig. 1a and Supplementary Figure 4. These obtained silver

chains are discrete but bridged to each other by C≡C groups and C≡N groups of L1 ligands to form the final 3D structure of Ag_{22}-CBP, as shown in Fig. 1d.

Fig. 1 | Structural anatomy of Ag_{22}-CBP.

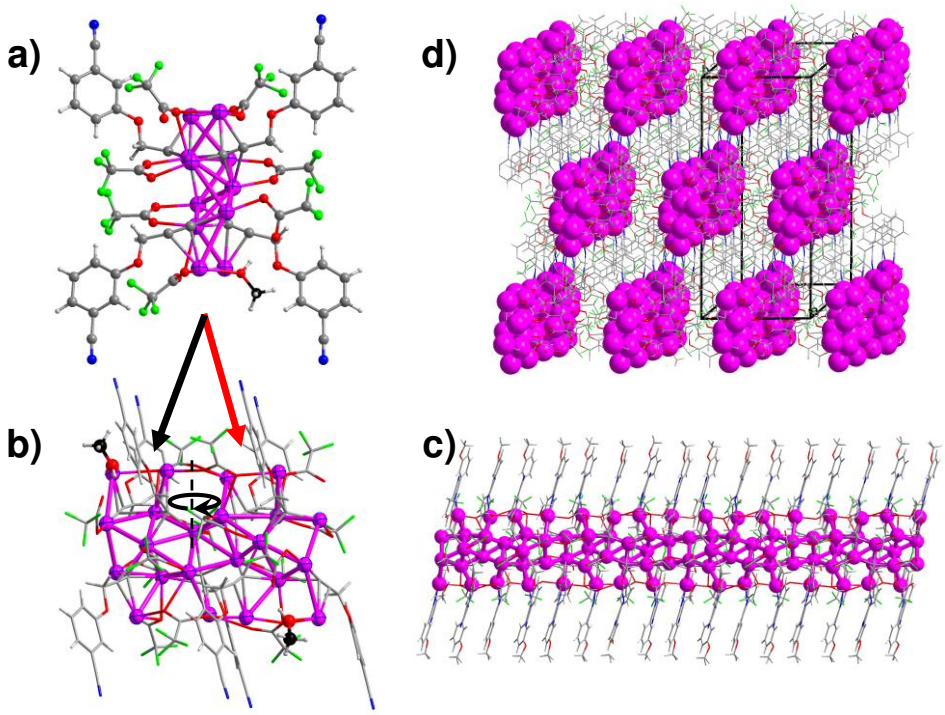

a The asymmetric structure of Ag_{22}-CBP. **b** The monomer structure of Ag_{22}-CBP. **c** 1D silver chain along ***c***-axis. **d** 3D structure. Color code: Ag, purple; F, cyan; O, red; N, blue; C, gray and black; H, white.

A 2D structure of Ag_{16}-CBP in *P-1* was obtained when the bidentate L1 ligand was replaced by the unidentate L2 ligand under the otherwise similar experimental conditions. As shown in Supplementary Figure 5, eight Ag atoms, nine $CF_3CO_2^-$ ions, one L2 ligand, two aqua molecules and one $[HNEt_3]^+$ are found in the minimum asymmetry unit. The S atom of L2 ligand bonds to five Ag atoms via Ag-S bonds (2.447(3)-2.979(2) Å) forming the main body of the inverted 6-figured Ag_6 unit as depicted in Figs. 2a and S6a, where the Ag-Ag bond length is in the range of 2.936(4)-3.043(3) Å. Furthermore, two Ag_6 units connect with each other generating a *Z*-motif Ag_{12} cluster (Fig. 2b and Supplementary Figure 7), which is covered by 14 trifluoroacetate ions via Ag-O bonds (2.215(3)-2.428(5) Å). A molecular cavity is formed

where two water molecules and one $[HNEt_3]^+$ ion settle down through Ag-O_{water} bonds of 2.481(5)-2.669(3) Å and hydrogen bond with a D---A distance of 2.798(3) Å between $[HNEt_3]^+$ ion and aquo molecule (Supplementary Figure 8). These Ag_{12} clusters are connected with each other by head to tail along ***b***-axis via (Ag_{12})-$O_{triflouroacetate}$-(Ag_{12}) motifs (Fig. 2c), where the shortest Ag---Ag distance between Ag_{12} clusters is ~ 3.572 Å, beyond the limit of Ag-Ag bond. Further, the $Ag_2(CF_3CO_2)_2$ units (noted as Ag_2, highlighted in green in Fig. 2 and Supplementary Figure 6b) serve as the linkers to connect neighboring Ag_{12} clusters in ***bc*** plane, i.e. the Ag_{12} clusters interact with four neighboring Ag_{12} clusters through four Ag_2 units by the (Ag_{12})-$O_{triflouroacetate}$-(Ag_2) motifs (Fig. 2c) to form a 2D plate. Finally, the 2D plates are packed into 3D structure through hydrogen bonds and Van Der Waals force between layers (Fig. 2d).

Fig. 2 | Structural anatomy of Ag_{16}-CBP.

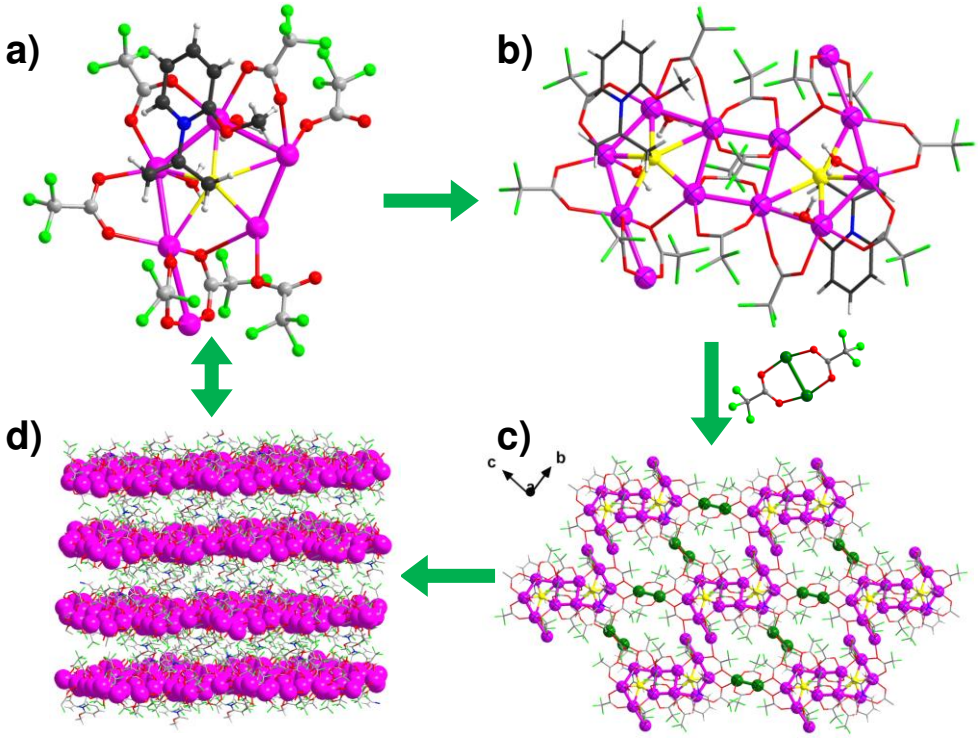

a Ag_6 unit in asymmetry. **b** Ag_{12} unit in monomer. **c** 2D structure and **d** 3D structure of Ag_{16}-CBP. Color code: Ag, purple and green; S, yellow; F, cyan; O, red; N, blue; C, grey and black; H, white.

Sensing response to alcohol. Different from the common silver complexes,[44] silver clusters[18,19] and even silver wires,[22] herein we have obtained the silver frameworks, silver chains in Ag_{22}-CBP and silver plates in Ag_{16}-CBP with unique and continuous features, which provide good channels for electrons to go through and prompt us to study their conductivity in the solid state.

We investigated the sensing property of the prepared 1D Ag_{22}-CBP chains and 2D Ag_{16}-CBP plates on a home-made setup in a clean-room at ambient temperature of ~ 24 °C. During the tests, the powder of Ag-CBPs was painted on a flexible PET board equipped with Cu wires giving a polymer film, which was further connected to a Source Meter 2450 forming a closed circle (Supplementary Figures 9-10). Initially, the films made of Ag_{22}-CBP and Ag_{16}-CBP samples were insulated under dry conditions as the reference. Once organic solvents (including protic solvents: methanol and ethanol, and aprotic solvents: acetone and toluene) were sprayed on the films, their conductivity differs, becoming conducting for methanol and ethanol, and insulating for acetone and toluene (Fig. 3 and Supplementary Figure 11). As shown in Figure 3a, the electric current turns to zero again with the removal of methanol or ethanol from the thin films under the irradiation of near-infrared light, indicating that the protic organic solvents should interact with Ag_{22}-CBP and Ag_{16}-CBP to make them conductive. On the contrary, the electric current was almost zero when the aprotic solvents, such as acetone or toluene, were sprayed on the sample films (Fig. 3a and Supplementary Figure 11), which corroborates that the Ag_{22}-CBP and Ag_{16}-CBP cannot detect these aprotic solvents, as the aprotic solvents cannot make the Ag_{22}-CBP and Ag_{16}-CBP nanomaterials conductive.

These different responses to organic solvents suggest that both Ag_{22}-CBP and Ag_{16}-CBP could serve as good sensors for the protic organic solvents (e.g., methanol and ethanol), like the nose to distinct and recognize different smells in air. The Ag_{22}-CBP and Ag_{16}-CBP nanomaterials showed excellent dynamic response to the methanol and ethanol detection, which is due to the robust nature of these Ag-CBP nanomaterials. It is worthy to note that the responding electric current to methanol is ~ 15 to 25-fold that of the ethanol detection, and the responding time for methanol is longer as well (Supplementary Figures

11-12), suggesting that the interaction between methanol and Ag_{22}-CBP or Ag_{16}-CBP is much stronger than that with ethanol, which could be further confirmed by the fact that the small holes in Ag_{22}-CBP and Ag_{16}-CBP formed by the surface ligands of silver frameworks are suitable for small molecules like methanol and water only.

Fig. 3 | Dynamic response and recovery characterization of artificial intelligent Ag-CBP sensors.

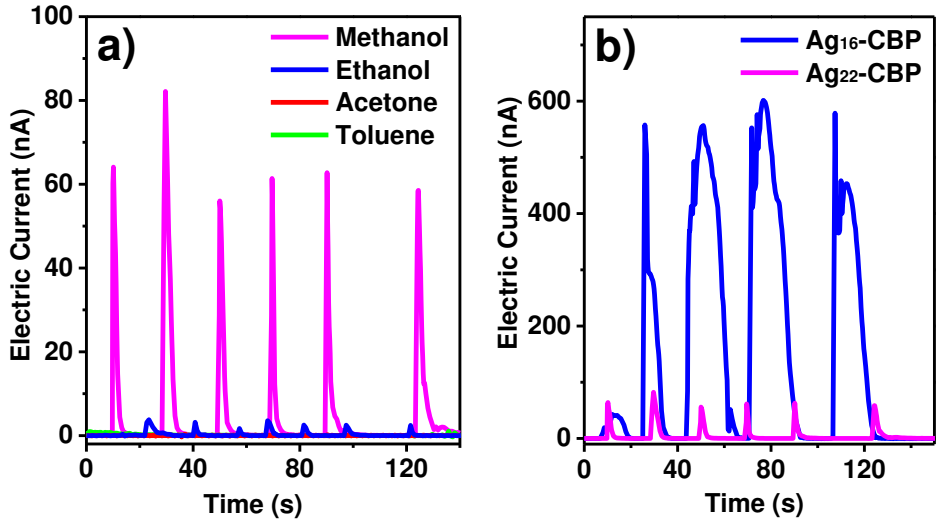

a Dynamic response and recovery curves of Ag_{22}-CBP thin film sensor under different organic solvents (protic solvents: methanol and ethanol; aprotic solvents: acetone and toluene). **b** Dynamic response and recovery curves of Ag_{22}-CBP and Ag_{16}-CBP films in the presence of methanol. All the sprays were measured at 0.1 V bias.

Furthermore, the current intensity of the Ag_{16}-CBP film (about 600 nA) is ~ ten-fold that of the Ag_{22}-CBP film (~ 60 nA) under the identical experimental conditions (Fig. 3b), though the recovery time of Ag_{16}-CBP film (~ 20 s) is much longer than that of Ag_{22}-CBP film (~ 5 s). All these results suggest that the Ag_{16}-CBP film is much more sensitive to methanol than the Ag_{22}-CBP film, which should be caused by the methanol absorption capability of the sensing material, for which the factors including the high-density Ag atoms arrangement, rich hydrogen bonds, ion features, and the mass transfer in the 2D film of the Ag_{16}-CBP should be responsible.

Titivate mechanism. The sensitivity to solvents of sensors is closed to the conductivity of Ag-CBP materials with solvents. Compared with the silver chains (1D) (Fig. 4a) in Ag_{22}-CBP, the silver planes (2D) (Fig. 4b) in Ag_{16}-CBP are more convenient for electrons to transfer in solid state where free electrons serve as the carriers and often move along a specific direction under the applied voltage, generating a current. Furthermore, the positive pyridine rings and $[HNEt_3]^+$ in Ag_{16}-CBP are helpful for the transformation of free electrons, beside the silver planes. In fact, the dry Ag-CBP powders are insulator since the silver chains in Ag_{22}-CBP and the silver planes in Ag_{16}-CBP are disconnected like a mess of broken electric wires, and no current can be generated even the voltage was applied. However, once the Ag-CBP powders get wet by some solvents, such as methanol, countless micro-electrolytic tanks (deep colored areas in Fig. 4) are formed among broken silver chains and plans in Ag-CBPs, where ions dissociated from the Ag-CBPs work as carriers in the electrolyte solution. Therefore, the sensitivity to solvents of sensors made of Ag-CBPs depends on the conductivity of micro-electrolytic tanks among silver chains and planes in Ag-CBP nanomaterials as the charge transformation in solid of Ag-CBPs is immune from solvents outside.

Fig. 4 | Titivate mechanism of the charge transformation in the Ag-CBPs.

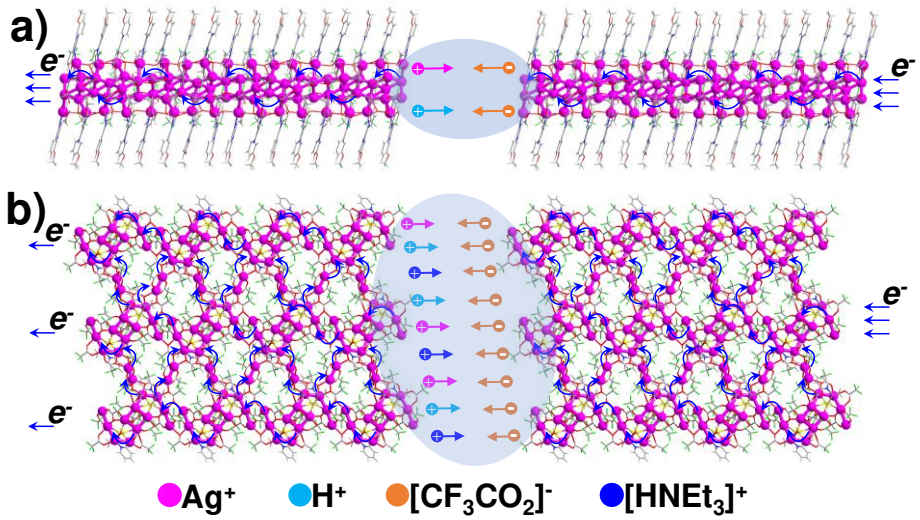

Charge transformation intra and inter **a** 1D silver chain of Ag_{22}-CBP and **b** 2D Ag_{16}-CBP film. Notes: Ag^+, purple ball; H, light blue ball; $[CF_3CO_2]^-$, orange ball; $[HNEt_3]^+$, blue ball; micro-electrolytic tanks, deep colored areas.

The saturated methanol solutions of Ag_{22}-CBP and Ag_{16}-CBP were used to simulate micro-electrolytic tanks between silver chains (1D) in Ag_{22}-CBP and the silver planes (2D) in Ag_{16}-CBP, respectively. The conductivity of saturated methanol solution of Ag_{16}-CBP was determined as 608 μS cm^{-1}, ~ 3 fold over that of Ag_{22}-CBP (228 μS cm^{-1}), indicating the micro-electrolytic tanks among silver planes in Ag_{16}-CBP showed better conductivity than that among silver chains in Ag_{22}-CBP. For the better conductivity of Ag_{16}-CBP in solution, the following structural factors may be responsible: (i) In species of carriers, Ag^+, $CF_3CO_2^-$, $[HNEt_3]$ species and even H^+ or $[H_3O]^+$ in Ag_{16}-CBP could serve as carriers in solution, but only Ag^+ and $CF_3CO_2^-$ could be disassociated from Ag_{22}-CBP and serve as carriers in solution. (ii) In the coordination models of Ag, all the Ag^+ cations were limited around L1 ligands through strong σ- and π-bonds, which is hard for Ag^+ to disassociate; while the $Ag_2(CF_3CO_2)$ units are free in Ag_{16}-CBP except the Ag^+ ions bonded to L2 ligand via Ag-S bond. (iii) The ligated waters and $[HNEt_3]^+$ ions in Ag_{16}-CBP could provide more H^+ ions, which are the fastest ionic carrier (mass transfer) in solution till now. All of these structural factors determine the superior conductivity of Ag_{16}-CBP in solution and more sensitive response to methanol. Furthermore, the conductivity of Ag-CBPs in ethanol was measured as ~ 50 μS cm^{-1}, ~ 0.45 μS cm^{-1} in acetone, and near zero μS cm^{-1} in toluene, which could well explain the weak electron response to ethanol and null to acetone and toluene.

Discussion

In summary, we have designed and prepared two novel nanocluster-based polymers, comprised of Ag nanoclusters linked with each other. Their crystal structures are determined by X-ray diffraction, which indicates that the coordination modes of ligands have an important influence on the self-assembly of cluster-based materials. Furthermore, the conductivity of the two polymers in the solid state could be

altered through organic solvents. Interestingly, the electric response to methanol is found on the Ag cluster-based polymers, suggesting the cluster-based materials may be used to design artificial intelligent sensors to detect organic solvents, especially methanol. Finally, we discussed the plausible mechanism of how the cluster-based materials work as a sensor to detect organic solvents in the presence of ambient atmosphere. This study on the synthesis and application of cluster-based materials enriches the artificial intelligent application of metal nanoclusters.

Methods

Synthesis of Ag_{22}-CBP and Ag_{16}-CBP.

All the operations were carried out in dark. Generally, 10 mg of Ag-L1 was dispersed into 5 mL MeOH, followed by the addition of $AgCO_2CF_3$ (88 mg 0.4 mmol) dissolved into 5 mL MeOH generating a white suspension. After 20 minutes later, a light-yellow solution was obtained from the mixture through filtration, which was then exposed to ethyl ether to crystalize in dark in ice refrigerator. The clear yellow block crystals of $\{Ag_{22}(L1)_8(CO_2CF_3)_{14}(CH_3OH)_2\}_n$ (denoted as Ag_{22}-CBP) were obtained in a few weeks.

Ag_{16}-CBP was obtained in a similar procedure. 10 mg Ag-L2 was dispersed into 5 mL MeOH was used in the preparation of Ag_{16}-CBP. The light-yellow plate crystal of $\{[Ag_{12}(L2)_2(CO_2CF_3)_{14}(H_2O)_4(AgCO_2CF_3)_4](HNEt_3)_2\}_n$ (denoted as Ag_{16}-CBP) was obtained after weeks in dark in ice refrigerator. The synthetic yields of Ag_{16}-CBP and Ag_{22}-CBP were 87% and 79%, respectively.

Sensor fabrication. For the preparation of cluster thin film sensor, 30 mg of the synthesized cluster-based materials were firstly dispersed in 5 mL of ethanol and then, the 5 mL of hydroxyl propyl methyl cellulose (HPMC) aqueous solution (4 mg mL^{-1}) was added to improve the viscosity. Next, 3 mL of cluster mixed solution obtained from the previous step was dripped on PET and dried at 60 ^oC in the oven for 10 min. Finally, the Cu wires were attached to the two ends of the film for providing the connection to the power supply.

The conductivity of samples in solution was determined by a DDS-307 conductivity meter. Crystal samples were dispersed into different solution and then filtrated with pinhole membrane filter generating saturated solutions to be tested. Before measurement, the conductivity meter was calibrated by stander solution of 1408 μs/cm.

Data Availability

The X-ray crystallographic coordinates for structures reported in this study have been deposited at the Cambridge Crystallographic Data Centre (CCDC), under deposition numbers 2111374 and 2111687. These data can be obtained free of charge from The Cambridge Crystallographic Data Centre via www.ccdc.cam.ac.uk/data_request/cif. The datasets generated and/or analyzed during this study are available from the corresponding author upon reasonable request.

References

1. Hamburg, M. A. Advancing regulatory science. *Science* **331**, 987 (2011).
2. Akamatsu, M., Mori, T., Okamoto, K., Komatsu, H., Kumagai, K., Shiratori, S., Yamamura, M., Nabeshima, T., Sakai, H., Abe, M., Hill, J. P., Ariga, K. Detection of ethanol in alcoholic beverages or vapor phase using florescent molecules embedded in a nano fibrous polymer. *ACS Appl. Mater. Inter.* **7**, 6189-694 (2015).
3. Jain, R., Tiwari, N., Prajapati, D. K., Upadhyay, A., Yadav, M. Car accident prevention using alcohol sensor. proceedings of second international conference on smart energy and communication. Algorithms for intelligent systems. *Springer, Singapore*, 619-623 (2021).
4. Jones, A.W. Alcohol, its analysis in blood and breath for forensic purposes, impairment effects, and acute toxicity. *Wires Forensic Sci.* **1**, e1353 (2019).
5. Araujo, W. R., Cardoso, T.M.G., Rocha, R. G., Santana, M. H. P., Munoz, R. A. A., Richter, E. M., Paixão, T.R.L.C., Coltro, W.K.T. Portable analytical platforms for forensic chemistry: A review. *Analytica Chimica Acta* 1034, 1-21 (2018).

6. Boroujerdi, R., Abdelkader, A., Paul, R. State of the art in alcohol sensing with 2D materials. *Nano-Micro Lett.* **12**, 33 (2020).
7. Malik, R., Tomer, V. K., Mishra, Y. K., Lin, L. Functional gas sensing nanomaterials: a panoramic view. *Appl. Phys. Rev.* **7**, 021301 (2020).
8. Ashmadvand, M., Zad, A.I., Mohammadpour, R., Hosseini-Shokouh, S. H., Asadian, H. Room temperature and high response ethanol sensor based on two-dimensional hybrid nanostructures of WS2/GONRs. *Sci. Rep.* **10**, 14799 (2020).
9. Thangamani, G .J., Deshmukh, K., Chidambaram, K,, Ahamed, M. B., Sadasivuni, K. K., Ponnamma, D., Faisal, M., Nambiraj, N. A., Pasha, S. K. K. Infuence of CuO nanoparticles and graphene nanoplatelets on the sensing behaviour of poly(vinyl alcohol) nanocomposites for the detection of ethanol and propanol vapors. *J. Mater. Sci.: Mater. Electron.* **29**, 5186-5205 (2018).
10. Lipatov, A., Varezhnikov, A., Wilson, P., Sysoev, V., Kolmakov, A., Sinitskii, A. Highly selective gas sensor arrays based on thermally reduced graphene oxide. *Nanoscale* **5**, 5426-5434 (2013).
11. Zhang, C., Hou, Z. L., Zhang, B.X., Fang, H.M., Bi, S. High sensitivity self-recovery ethanol sensor based on polyporous graphene oxide/melamine composites. *Carbon* **137**, 467-474 (2018).
12. Chen, D., Hou, X., Wen, H., Wang, Y., Wang, H., Li, X., Zhang, R., Lu, H., Xu, H., Guan, S., Sun, J., Gao, L. The enhanced alcohol-sensing response of ultrathin WO_3 nanoplates. *Nanotechnology* **21**, 035501 (2010).
13. Jing, Z., Zhan, J. Fabrication and gas-sensing properties of porous ZnO nanoplatlets. *Adv. Mater.* **20**, 4547-4551. (2008).
14. Li, X. J., Chen, S.J., Feng, C.Y. Characterization of silicon nanoporous pillar array as room-temperature capacitive ethanol gas sensor. *Sens. Actuators B* **123**, 461–465 (2007).
15. Muangrat, W., Wongwiriyapan, W., Morimoto, S., Hashimoto, Y. Graphene nanosheet-grafted double-walled carbon nanotube hybrid nanostructures by two step chemical vapor deposition and their application for ethanol detection. *Sci. Rep.* **9**, 7871 (2019).

16. Vandezande, W., Janssen, K. P. F., Delport, F., Ameloot, R., Vos, D. E. D., Lammertyn, J., Roeffaers, M. B. J. Parts per million detection of alcohol vapors via metal organic framework functionalized surface plasmon resonance sensors. *Anal. Chem.* **89**, 4480–4487（2017).
17. Sharma, A. K., Dominic, A. Fluoride fiber-optic SPR sensor with graphene and NaF layers: Analysis of accuracy, sensitivity, and specificity in near infrared. *IEEE Sens. J.* **18**, 4053-4058 (2018).
18. Jin, R., Li, G., Sharma, S., Li, Y., Du, X. Toward active-site tailoring in heterogeneous catalysis by atomically precise metal nanoclusters with crystallographic structures. *Chem. Rev.* **121**, 567-648. (2021).
19. Chakraborty, I., Pradeep, T. Atomically precise clusters of noble metals: Emerging link between atoms and nanoparticles. *Chem. Rev.* **117**, 8208-8271 (2017).
20. Shi, Q., Qin, Z., Sharma, S., Li, G. Recent progress in heterogeneous catalysis by atomically and structurally precise metal nanoclusters. *Chem. Rec.* DOI: 10.1002/tcr.202100001 (2021).
21. Kawawaki, T., Ebina, A., Hosokawa, Y., Ozaki, S., Suzuki, D., Hossain, S., Negishi, Y. Thiolate-protected metal nanoclusters: recent development in synthesis, understanding of reaction, and application in energy and environmental field. *Small* DOI: 10.1002/smll.202005328 (2021).
22. . Luo, Z., Zheng, K., Xie, J. Engineering ultrasmall water-soluble gold and silver nanoclusters for biomedical applications. *Chem. Commun.* **50**, 5143-5155 (2014).
23. An, Y., Ren, Y., Bick, M., Dudek, A., Waworuntu H-W. E., Tang, J., Chen, J., Chang, B. Highly fluorescent copper nanoclusters for sensing and bioimaging. *Biosens. bioelectron.* **154**, 112078 (2020).
24. Qiao, Z., Zhang, J., Hai, X., Yan, Y., Song, W., Bi, S. Recent advances in templated synthesis of metal nanoclusters and their applications in bosensing, bioimaging and theranostics. *Biosens. Bioelectron.* **176**, 112898. (2021).

25. Hossain, S., Imai, Y., Motohashi, Y., Chen, Z., Suzuki, D., Suzuki, T., Kataoka, Y., Hirata, M., Ono, T., Kurashige, W., Kawawaki, T., Yamamoto, T., Negishi, Y. Understanding and designing one-dimensional assemblies of ligand-protected metal nanoclusters. *Mater. Horiz.* **7**, 796-803 (2020).
26. Ebina, A., Hossain, S., Horihata, H., Ozaki, S., Kato, S., Kawawaki, T., Negishi, Y. One-, two-, and three-dimensional self-assembly of atomically precise metal nanoclusters. *Nanomaterials* **10**, 1105 (2020).
27. Yuan, P., Zhang, R., Selenius, E., Ruan, P., Yao, Y., Zhou, Y., Malola, S., Häkkinen, H., Teo, B.K., Cao, Y., Zheng, N. Solvent-mediated assembly of atom-precise gold-silver nanoclusters to semiconducting one-dimensional materials. *Nat. Commun.* **11**, 2229 (2020).
28. Nardi, M.D., Antonello, S., Jiang, D.-E., Pan, F., Rissanen, K., Ruzzi, M., Venzo, A., Zoleo, A., Maran, F. Gold nanowired: A linear $(Au_{25})_n$ polymer from Au_{25} molecular clusters. *ACS Nano* **8**, 8505-8512 (2014).
29. Wu, Z., Yao, Q., Zang, S., Xie, J. Directed self-assembly of ultrasmall metal nanoclusters. *ACS Materials Lett.* **1**, 237-248 (2019).
30. Chen, Z.-Y., Tam, D.Y.S., Zhang, L.L.-M., Mak, T.C.W. Silver thiolate nano-sized molecular clusters and their supramolecular covalent frameworks: An approach toward pre-templated synthesis. *Chem. Asian J.* **12**, 2763-2769（2017).
31. Wang, Z. Y., Wang, M. Q., Li, Y. L., Luo, P., Jia, T. T., Huang, R. W., Zang, S. Q., Mak, T. C. W., Atomically precise site-specific tailoring and directional assembly of superatomic silver nanoclusters. *J. Am. Chem. Soc.* **140**, 1069-1076 (2018).
32. Mak, T. C., Zhao, L., Multinuclear silver ethynide supramolecular synthons for the construction of coordination networks. *Chem. Asian. J.* **2**, 456-67 (2007).
33. Li, X.-Y., Su, H.-F., Xu, J. A 2D Layer network assembled from an open dendritic silver cluster $Cl@Ag_{11}N_{24}$ and an N-donor ligand. *Inorg. Chem. Front.* **6**, 3539-3544 (2019).

34. Huang, R.-W., Dong, X.-Y., Yan, B.-J., Du, X.-S., Wei, D.-H., Zang, S.-Q., Mak, T.C.W. Tandem silver cluster isomerism and mixed linkers to modulate the photoluminescence of cluster-assembled materials. *Angew. Chem. Int. Ed.* **57**, 8560-8566 (2018).

35. Alhilaly, M.J., Huang, R.-W., Naphade, R., Alamer, B., Hedhili, M.N., Emwas, A.-H., Maity, P., Yin, J., Shkurenko, A., Mohammed, O.F., Eddaoudi, M., Bakr, O. M. Assembly of atomically precise silver nanoclusters into nanocluster-based frameworks. *J. Am. Chem. Soc.*, **141**, 9585-9592 (2019).

36. Wang, Z., Sun, Y.-M., Qu, Q.-P., Liang, Y.-X., Wang, X.-P., Liu, Q.-Y., Kurmoo, M., Su, H.-F., Tung, C.-H., Sun, D. Enclosing classical polyoxometallates in silver nanoclusters. *Nanoscale* **11**, 10927-10931 (2019).

37. Zhao, M., Huang, S., Fu, Q., Li, W., Guo, R., Yao, Q., Wang, F., Cui, P., Tung, C. H., Sun, D., Ambient chemical fixation of CO_2 using a robust Ag_{27} cluster-based two-dimensional metal-organic framework. *Angew. Chem. Int. Ed.* **59**, 20031-20036 (2020).

38. Chen, S., Du, W., Qin, C., Liu, D., Tang, L., Liu, Y., Wang, S., Zhu, M. Assembly of the thiolated $[Au_1Ag_{22}(S\text{-}Adm)_{12}]^{3+}$ superatom complex into a framework material through direct linkage by SbF_6^- anions. *Angew. Chem. Int. Ed.* **59**, 7542-7547 (2020).

39. Lei, Z., Pei, X.-L., Jiang, Z.-G., Wang, Q.-M. Cluster linker approach: preparation of a luminescent porous framework with NbO topology by linking silver ions with gold(I) clusters. *Angew. Chem. Int. Ed.* **53**, 12771-12775 (2014).

40. Wu, X.-H., Luo, P., Wei, Z., Li, Y.-Y., Huang, R.-W., Dong, X.-Y., Li, K., Zang, S.-Q., Tang, B.Z. Guest-triggered aggregation-induced emission in silver chalcogenolate cluster metal-organic frameworks. *Adv. Sci.* **6**, 1801304 (2019).

41. Wei, Z., Wu, X.-H., Luo, P., Wang, J.-Y., Li, K., Zang, S.-Q. Matrix coordination induced emission in a three-dimensional silver cluster-assembled material. *Chem. Eur. J.* **25**, 2750-2756 (2019).

42. Huang, R.-W., Wei, Y.-S., Dong, X.-Y., Wu, X.-H., Du, C.-X., Zang, S.-Q., Mak, T.C.W. Hypersensitive dual-function luminescence switching of a silver-chalcogenolate cluster-based metal-organic framework. *Nat. Chem.* **9**, 689-697 (2017).

43. Wang, Z. Y. et al. Atomically precise site-specific tailoring and directional assembly of superatomic silver nanoclusters. *J. Am. Chem. Soc.* **140**, 1069-1076（2018).

44. Z. Wang, N. V. Tzouras, S. P. Nolan, X. Bi, Silver N-heterocyclic carbenes: emerging powerful catalysts. *Trend. Chem.* **3**, 674-685 (2021).

Acknowledgements

We acknowledged the financial support by Natural Science Foundation of China (2217020878) and Liaoning Natural Science Foundation of China (2020-MS-024).

Ethics declarations

Competing interests

The authors declare no competing interests.

Supplementary Information

- Supplementary Figures 1–12.

Supplementary Files

This is a list of supplementary files associated with this preprint. Click to download.

- checkcifofAg16CBP.pdf
- checkcifforAg22CBP.pdf
- Ag16CBP.cif
- Ag22CBP.cif
- SupplementaryInformation.pdf